Ocean-based Negative Emission Technologies

OCEAN NETs

Deliverable Title	**Deliverable 4.8: Report on carbon cycle interactions and efficacy of land-based CDRs (e.g. BECCS), when combined with oceanic CDRs (individually or in a portfolio)**
Lead	NTNU
Related Work Package	WP4
Related Task	Task 4.6
Author(s)	Helene Muri, Anusha Sathyanadh
Prieto Dissemination Level	Public
Due Submission Date	30.06.2024
Actual Submission	08.07.2024
Project Number	869357
Start Date of Project	01. January 2022
Duration	60 months

Abstract:
In this deliverable 4.8, we analyze the Norwegian Earth System Model (NorESM) simulations from Deliverable 4.6 and 4.7 on land-based and ocean-based Carbon Dioxide Removal (CDR) scenarios. We focus the analysis on BioEnergy coupled to CCS (BECCS) using sugarcane as feedstock, and ocean alkalinity enhancement (OAE), applied individually and in combinations. We find that a higher amount of carbon captured by making use of the carbon sequestration potential of land and ocean together, as expected. The sugarcane yield is unaffected by the OAE deployment, however, carbon uptake by other parts of the land is somewhat reduced by OAE in the combined BECCS and OAE case. Less carbon is taken up by the oceans during BECCS deployment, whilst less carbon is taken up by land during the OAE deployment. The uptake of carbon by the oceans in the combined BECCS and OAE case is directly additive from the individual cases. However, some non-linear responses are seen in other parts of the climate responses.

This project has received funding from the European Union's Horizon 2020 research and innovation programme under grant agreement number 869357.

Document History

Date	Version	Description	Name/Affiliation
28.06.2024	1.0	First submitted version.	Helene Muri

Disclaimer:

This document reflects only the author's view and the European Commission, and their executive agency are not responsible for any use that may be made of the information it contains.

List of abbreviations, acronyms, and definitions

CDR	Carbon dioxide removal
NET	Negative emission technology
BECCS	Bio-Energy with Carbon Capture and Storage
OAE	Ocean alkalinity enhancement
SSP5-3.4-OS	Shared Socio-Economic Pathway 5-3.4 Overshoot
CMIP6	Coupled Model Intercomparison Project Phase 6
ESM	Earth System Model
IPCC	Intergovernmental Panel on Climate Change
BLOM	Bergen Layered Ocean Model
CaO	Calcium Oxide
ESM	Earth System Models
EEZ	Exclusive Economic Zones

List of figures

Figure 1: Time series of area (million km^2) covered by sugarcane (sum of tropical and temperate) in the SSP5-3.4OS dataset and the modified SSP5-3.4 sugarcane dataset.

Figure 2: Distribution of additional sugarcane area in the modified land use dataset used for the BECCS simulation (km^2).

Figure 3: Area covered by the most widely used types of crops, where rainfed and irrigated varieties of each crop are summed, and the area increase (million km^2) in 2100 compared to 2015 is plotted for both the original SSP5-3.4-OS (yellow) and the modified land use (green).

Figure 4: a) Anthropogenic CO_2 emissions (kg m^{-2} s^{-1}) in the three simulations; SSP5-3.4-OS (blue), BECCS (green), BECCS-OAE (orange), and b) Difference in global anthropogenic CO_2 emissions in the BECCS and BECCS-OAE scenarios compared to the SSP5-3.4-OS scenario.

Figure 5: OAE application of CaO in year 2100, assuming CaO deployment in the uppermost ocean layer inside the Exclusive Economic Zones (EEZ) of the three regions (US, EU, and China). For each region, the annual deployed amount of CaO is distributed evenly and defined as added alkalinity in mol m^{-2} s^{-1}.

Figure 6: Comparison of annual mean atmospheric CO_2 mixing ratio (ppmv): (a) Timeseries of absolute values (black dashed: SSP5-3.4-OS, green: BECCS, blue: OAE, orange: BECCS-OAE), and (b) Difference in mixing ratio compared to the baseline simulation.

Figure 7: Comparison of (a) 12-year Rolling Mean Global Average Atmospheric Near Surface Temperature (2030-2100), and (b) Reduction in temperature with respect to the baseline, *SSP5-3.4-BECCS* simulation.

Figure 8: Spatial distributions of annual mean near surface air temperature changes (°C) over the last part of the century, 2070–2100, for *SSP5-3.4-OAE*, *SSP5-3.4-BECCS* and *SSP5-3.4-BECCS-OAE* scenarios minus the SSP5-3.4 scenario.

Figure 9: Timeseries comparison of 12 year running mean Latent Heat Flux (LHF, W m^{-2}).

Figure 10: (a) 12-year running mean timeseries of projected uptake of global land NBP (CO_2 taken up by land, atmosphere-land CO_2 flux) in different simulations (PgC / year) (b) change in cumulative NBP with respect to the SSP5-3.4 simulation (PgC).

Figure 11: Spatial distributions of NBP (gC/m2/year) over the globe in long-term (2070–2100) periods under the SSP5-3.4-OAE, SSP5-3.4-BECCS and SSP5-3.4-BECCS-OAE scenarios with respect to the SSP5-3.4 scenario.

Figure 12: Time series of NPP from each simulation (PgC / year) (a), and (b) cumulative change in NPP with respect to the SSP5-3.4 simulation (PgC).

Figure 13: Spatial distributions of NPP changes (gC/m2/year) over the period 2070–2100 for the *SSP5-3.4-OAE*, *SSP53.4-BECCS* and *SSP5-3.4-BECCS-OAE* scenarios compared to the SSP5-3.4 baseline scenario.

Figure 14: AGNPP from the additional sugarcane areas in the BECCS (green) and BECCS-OAE (orange) simulations (PgC / year).

Figure 15: Time series of (a) Gross primary production (PgC / year) (b) cumulative change in Gross primary production with respect to SSP5-3.4 (PgC), c) Ecosystem Respiration (PgC / year), and (d) cumulative change in ecosystem respiration compared to SSP5-3.4 (PgC).

Figure 16: Mean change in GPP (gC m^{-2} $year^{-1}$) over the years 2070–2100 in *SSP5-3.4-OAE*, *SSP5-3.4-BECCS* and *SSP5-3.4-BECCS-OAE* scenarios compared to the SSP5-3.4 scenario.

Figure 17: Timeseries comparison of (a) total vegetation carbon (PgC / year), and (b) change in cumulative total vegetation carbon with respect to SSP5-3.4 (PgC).

Figure 18: Comparison of (a) 12-year rolling mean global average sea surface temperature (°C), and (b) Difference in SST with respect to the baseline simulation SSP5-3.4.

Figure 19: Timeseries of air – sea flux of carbon in each simulation (PgC / year) (a), and the cumulative difference from SSP5-3.4 (PgC) (b).

Figure 20: Spatial distributions of changes to the air – sea carbon flux (gC m^{-2}) over the period of 2070–2100 for *SSP5-3.4-OAE*, *SSP5-3.4-BECCS* and *SSP5-3.4-BECCS-OAE* scenarios compared to the SSP5-3.4 scenario.

Figure 21: Comparison of (a) global mean pCO2 (μatm), and (b) cumulative change compared to the baseline simulation (μatm).

Figure 22: Spatial distributions of change in Surface Ocean pCO2 over the period of 2070–2100 for *SSP5-3.4-OAE*, *SSP5-3.4-BECCS* and *SSP5-3.4-BECCS-OAE* scenarios compared to SSP5-3.4.

List of tables

Table 1: Description of the NorESM2 simulations.

Table 2: Summary of global mean atmospheric variables.

Table 3: Summary of response in land variables at 2100, reduction relative to SSP534 baseline at 2100, cumulative differences, and 2070 – 2100 mean changes.

Table 4: Summary of ocean variables from the simulations, including the value at 2100, reduction relative to SSP534 baseline at 2100.

1. Introduction

1.1 Context

OceanNETs is a European Union project funded by the Commission's Horizon 2020 program under the topic of Negative emissions and land-use based mitigation assessment (LC-CLA-02-2019), coordinated by GEOMAR Helmholtz Centre for Ocean Research Kiel (GEOMAR), Germany.

OceanNETs responds to the societal need to rapidly provide a scientifically rigorous and comprehensive assessment of negative emission technologies (NETs). The project focuses on analyzing and quantifying the environmental, social, and political feasibility and impacts of ocean-based NETs. OceanNETs will close fundamental knowledge gaps on specific ocean-based NETs and provide more in-depth investigations of NETs that have already been suggested to have a high CDR potential, levels of sustainability, or potential co-benefits. It will identify to what extent, and how, ocean-based NETs can play a role in keeping climate change within the limits set by the Paris Agreement.

1.2 Purpose and scope of the deliverable

The purpose of this deliverable 4.8 is to analyze the carbon cycle interactions and efficacy of land-based (i.e. Bioenergy with carbon capture and storage, BECCS) and ocean-based CDRs, individually and in combination. The dataset provided by deliverables 4.6 and 4.7 are used for investigating the potential risks and benefits of large-scale global deployment of terrestrial and ocean BECCS together and independently using selected land and atmospheric variables.

1.3 Relation to other deliverables

D4.8 is making use of the 2030-high ocean alkalinity enhancement (OAE) simulation performed with NorESM2 in D4.6. The scenario design for 2030-high was informed by D6.2: Realistic deployment scenarios/pathways that can be used to constrain Earth System models. Information provided by WP5 and WP6 has informed the scenario design for the simulations analyzed in this deliverable. The OAE data will be further analyzed in D4.9, where the atmospheric and land responses to different ocean-based NETs will be compared.

2. Methodology and simulations with NorESM2

2.1 Model description

For the set of model simulations, we used the version of the coupled Norwegian ESM that contributed towards CMIP6 (Coupled Model Intercomparison Project phase 6), NorESM2-LM with 1° resolution in the ocean and ~2° resolution in the atmosphere and land components (Seland et al., 2020; Tjiputra et al., 2020). The model is open access and available here: (https://github.com/NorESMhub/NorESM/releases/tag/release-noresm2.0.6). As detailed in the D4.6 and D4.7 reports, the emission driven SSP5-3.4 scenario (Meinshausen et al., 2019) is the baseline for the experiments. For this version of the model, NorESM2.0.6, capabilities for OAE have been developed as part of the WP4 of OceanNETs. Four different NorESM2 simulations are listed

in Table 1 and described in more detail in the report D4.7. The simulations are described here in the WP4 protocol document as well, https://docs.google.com/spreadsheets/d/1GfcSaIJKeCtADxaLSqVPWqPXdrMXL7fXT5REnRhY7ws/edit#gid=0"https://docs.google.com/spreadsheets/d/1GfcSaIJKeCtADxaLSqVPWqPXdrMXL7fXT5REnRhY7ws/edit#gid=0

Table 1: Description of the NorESM2 simulations.

Experiment	Description	Years
SSP5-3.4	SSP5-3.4-OS CMIP6 simulation	2015- 2100
SSP5-3.4-OAE	SSP5-3.4 with 2030-high OAE scenario.	2030-2100
SSP5-3.4-BECCS	2015 area is kept for food and the increased cropland area is used for sugarcane from 2030 to 2100 and coupled to CCS.	2030-2100
SSP5-3.4-BECCS-OAE	SSP5-3.4 Sugarcane BECCS simulation combined with OAE	2030-2100

2.2 BECCS and OAE Scenarios

The land-based CDR simulation design is documented in the report of D4.7 (Sathyanadh and Muri, 2024). A brief summary is provided here. The terrestrial BECCS scenario is formulated by modifying the Community Land Model version 5 (CLM5) input land use distribution data (Lawrence et al., 2019). Each grid cell can have a different number of land units, each land unit can have a different number of columns, and each column can have multiple patches each with a specific plant functional type (PFT) or crop functional type (CFT).

The original CMIP6 SSP5-3.4-OS land use timeseries has been modified to change the crop distribution in such a way that the total crop area for 2015 is kept for food throughout the century and the increase in crop area of other crops from 2016 until 2100 is used for planting more sugarcane. We chose sugarcane as the most suitable crop as it has the highest crop area expansion in the original CMIP6 SSP5-3.4-OS owing to its use for bioenergy generation and because of its high potential yield. There is an increase of 5.1 million km² additional sugarcane area in the modified SSP5-3.4-OS land use file by the end of the century (Fig. 1). The increased sugarcane areas are mostly in Sub-Saharan region, in the South American east coast, and in the mid-east North America (Fig. 2). Sugarcane replaced the areas prominently covered by rice, spring wheat, tropical corn, and fodder grass (Fig. 3).

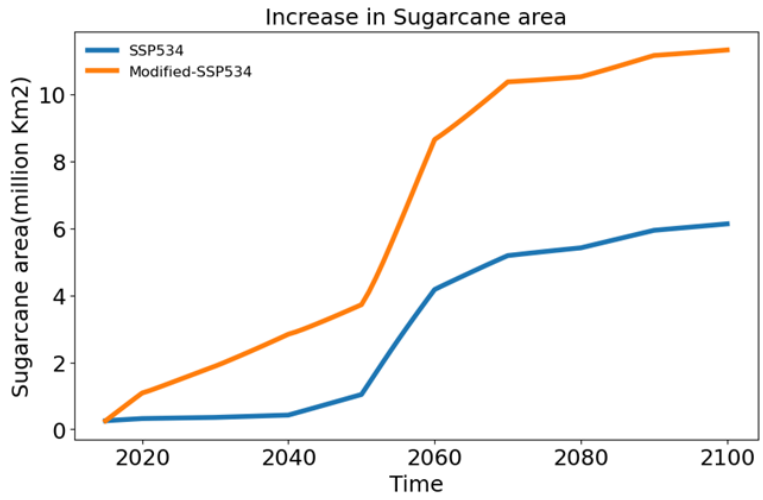

Figure 1: Time series of area (million km²) covered by sugarcane (sum of tropical and temperate) in the SSP5-3.4OS dataset and the modified SSP5-3.4 sugarcane dataset.

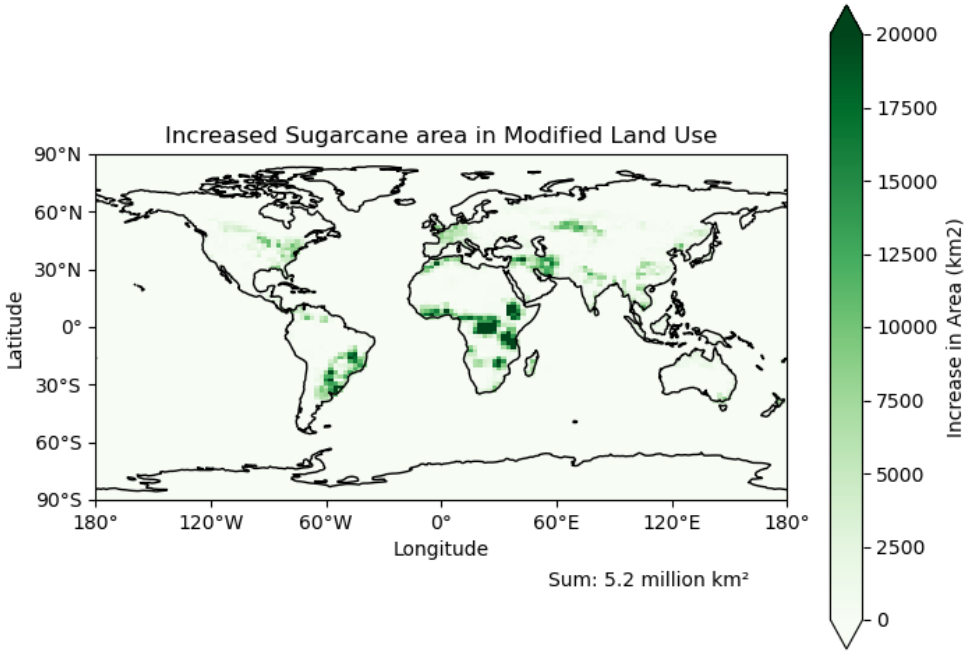

Figure 2: Distribution of additional sugarcane area in the modified land use dataset used for the BECCS simulation (km²).

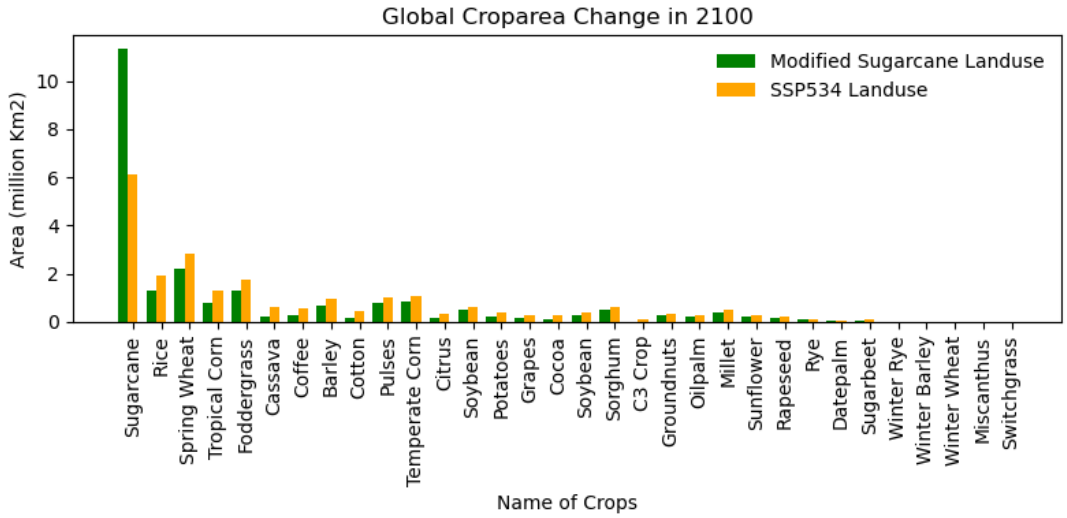

Figure 3: Area covered by the most widely used types of crops, where rainfed and irrigated varieties of each crop are summed, and the area increase (million km²) in 2100 compared to 2015 is plotted for both the original SSP5-3.4-OS (yellow) and the modified land use (green).

We also applied Carbon capture and Storage (CCS) for the bioenergy production system. We have further developed the CCS code from NorESM1-ME (Muri, 2018) to NorESM2 with an updated conversion efficiency based on recent literature on sugarcane bioenergy production systems. As bioenergy is replacing fossil energy within the model, there is a net reduction in CO_2 emissions, as seen in Fig. 4.

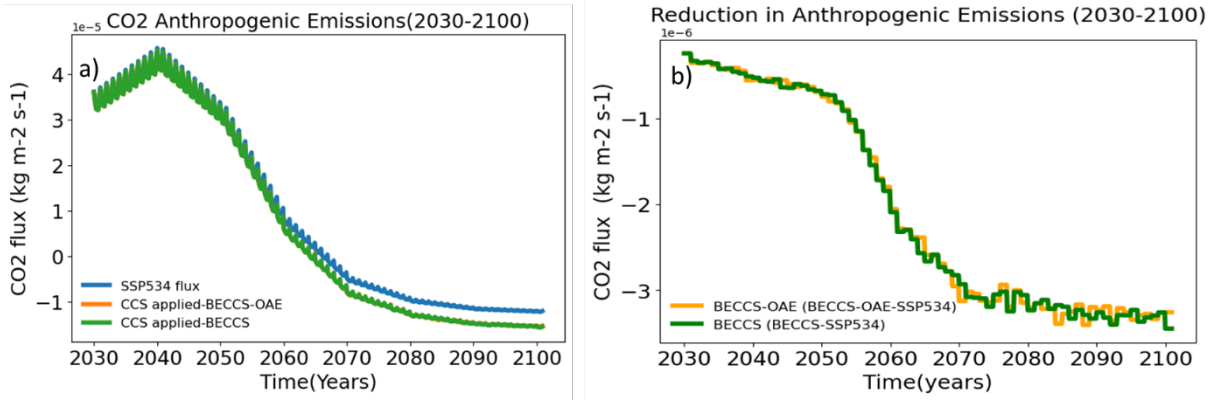

Figure 4: a) Anthropogenic CO_2 emissions (kg m^{-2} s^{-1}) in the three simulations; SSP5-3.4-OS (blue), BECCS (green), BECCS-OAE (orange), and b) Difference in global anthropogenic CO_2 emissions in the BECCS and BECCS-OAE scenarios compared to the SSP5-3.4-OS scenario.

In the OAE scenario used for this study is *2030-high*, as described in D4.6 (Partanen and Bergman, 2024), the alkalinity deployment is initiated in the year 2030 by dispersing CaO at the ocean surface in the exclusive economic zones (EEZ) of the US, Europe, and China. The fluxes in year 2100 can be seen in Fig. 5. These three regions are chosen based on the availability of current excess capacities of lime and cement industries. For each region, the annual deployed amount of CaO is distributed evenly and defined as added alkalinity in mol m^{-2} s^{-1}.

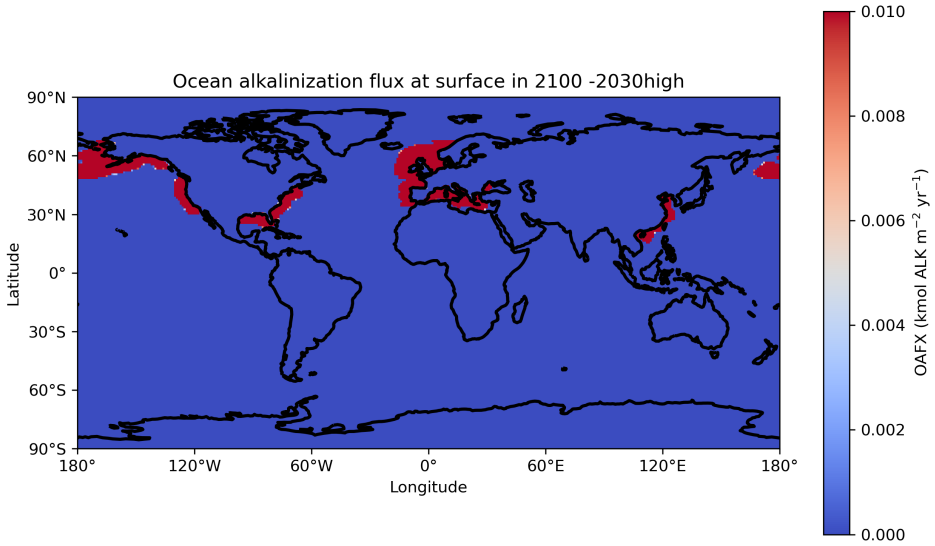

Figure 5: OAE application of CaO in year 2100, assuming CaO deployment in the uppermost ocean layer inside the Exclusive Economic Zones (EEZ) of the three regions (US, EU, and China). For each region, the annual deployed amount of CaO is distributed evenly and defined as added alkalinity in mol m^{-2} s^{-1}.

3. Results

3.1 Atmospheric response to CDR

The time series of atmospheric CO_2 mixing ratio reveals a consistent increase from 442 ppmv to around 545 ppmv in 2060, as expected from the SSP5-3.4-OS scenario (Meinshausen et al., 2020), followed by a gradual decline. Towards the end of the century, the CO_2 mixing ratio in all the CDR scenarios decreased considerably and are all lower than in SSP5-3.4-OS. The reduction in CO_2 concentrations is of up to 16 ppm by 2100, with the BECCS and OAE combined simulations seeing the largest reductions. SSP534-OAE has the lowest reduction of 7 ppm. The simultaneous SSP534-BECCS-OAE has a reduction of 23 ppm, which also corresponds to the a sum of the individual scenarios.

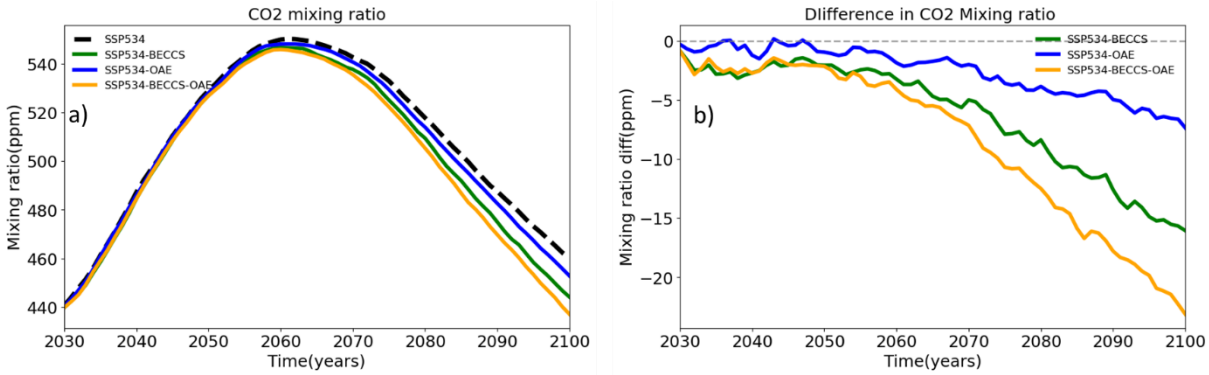

Figure 6: Comparison of annual mean atmospheric CO_2 mixing ratio (ppmv): (a) Timeseries of absolute values (black dashed: SSP5-3.4-OS, green: BECCS, blue: OAE, orange: BECCS-OAE), and (b) Difference in mixing ratio compared to the baseline simulation.

With regards to the temperature response, the simulation *SSP5-3.4-BECCS-OAE*, combining BECCS and OAE, and the *SSP5-34-BECCS* simulations both show a somewhat higher temperature in the beginning compared to SSP5-3.4 (Fig. 7). From the 2060s and onwards the temperatures are lower in all CDR simulations compared to SSP5-34. Over this period there is a significant increase in the CDR application and hence a stronger temperature response. The temperatures are lowered when the CO_2 concentrations are reduced by 5 ppm or more. During the first three decades of BECCS deployment, the biogeophysical feedbacks are dominating the biogeochemical feedbacks, whereupon the temperatures are somewhat increased by 0.1 – 0.2 °C, despite atmospheric CO_2 concentrations being lower. When the BECCS application area is doubled from about 5 to 10 million km^2, the temperatures are reduced to below the SSP5-3.4 range, but the cooling remains small throughout the simulation, despite the large scare deployment of BECCS. Combining OAE and BECCS results in a similar temperature response as when applying OAE alone. OAE is more effective at reducing the temperatures, as it avoids biogeophysical implications.

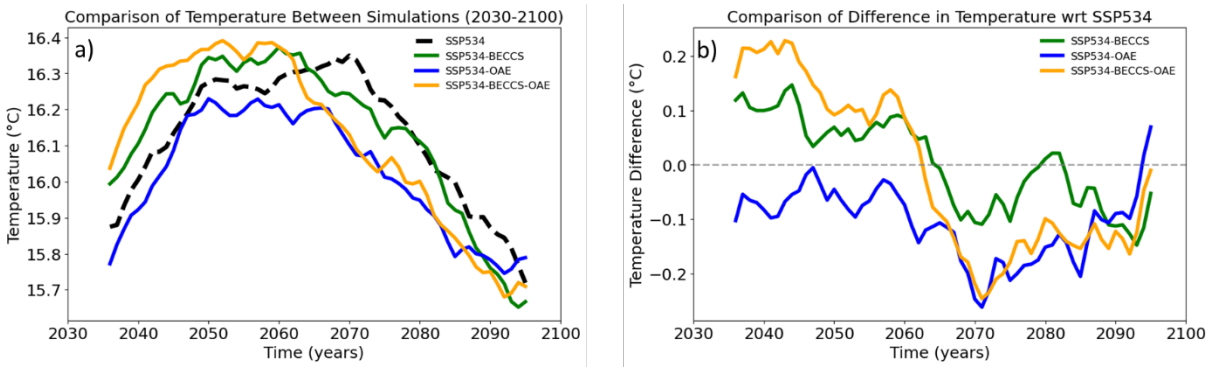

Figure 7: Comparison of (a) 12-year Rolling Mean Global Average Atmospheric Near Surface Temperature (2030-2100), and (b) Reduction in temperature with respect to the baseline, SSP5-3.4-BECCS simulation.

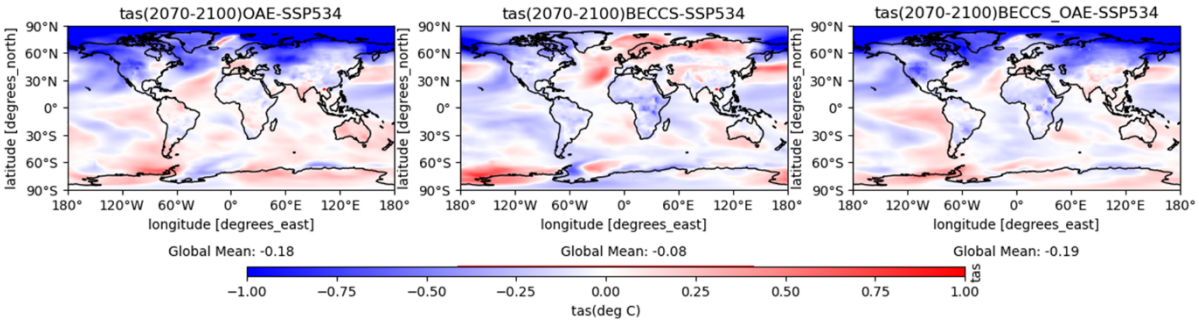

Figure 8: Spatial distributions of annual mean near surface air temperature changes (°C) over the last part of the century, 2070–2100, for SSP5-3.4-OAE, SSP5-3.4-BECCS and SSP5-3.4-BECCS-OAE scenarios minus the SSP5-3.4 scenario.

The changes to near surface air temperatures are mainly seen in the northern hemisphere (Fig. 8), where a cooling is largely seen. The SSP534-BECCS show some localized temperature changes in the regions where more biocrops have been introduced. The individual SSP534-OAE scenario, as well as the simultaneous SSP534-BECCS_OAE scenario, exhibit more pronounced cooling over the northern high latitude regions (exceeding 1.5°C), with slight warming observed over the oceans,

including in the ENSO (El Niño – Southern Oscillation) region. Any further changes to this climatic feature will be needed to be investigated in more detail in the future.

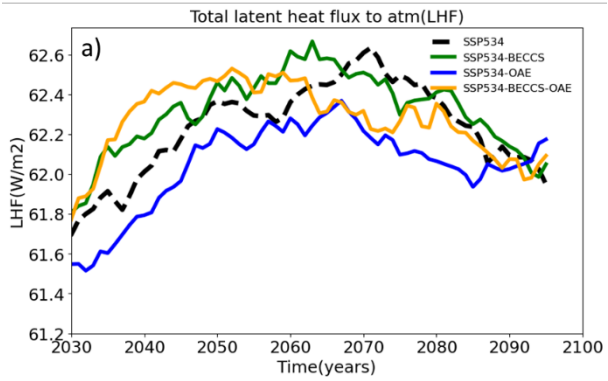

Figure 9: Timeseries comparison of 12 year running mean Latent Heat Flux (LHF, W m^{-2}).

The latent heat flux gradually increases from 2030 until 2070, and peaks around the same time as the global mean temperatures, and then gradually decreases in all scenarios (Fig. 9). The *SSP534-OAE* scenario follows *SSP534* and is consistently lower by about 0.2 – 0.3 W m^{-2} (see also Table 2), as is expected with forcing being applied over the ocean with a more homogenous reduction in temperatures compared to the land-based CDR.

Table2: Summary of global mean atmospheric variables.

Variable	Simulation	2100 value
CO_2 concentrations (ppmv)	**SSP534**	**460**
	BECCS	**444**
	OAE	**452**
	BECCS-OAE	**437**
Temperature (°C)	**SSP534**	**15.5**
	BECCS	**15.7**
	OAE	**15.8**
	BECCS-OAE	**15.6**
Latent heat (Wm^{-2})	**SSP534**	**61.6**
	BECCS	**62.4**
	OAE	**61.2**
	BECCS-OAE	**62.3**

As for the BECCS and BECCS plus OAE combined simulations, there is predominantly an increase in latent heat flux due to the changes in the crop type to sugarcane. More energy is being transferred to the atmosphere through these land surface property changes. During the latter part of the century when the BECCS application is significantly ramped up, the reductions in temperatures are affecting the latent heat flux, whereupon it becomes more or less the same in the *SSP534*, *SSP534-BECCS* and *SSP534-BECCS-OAE* simulations.

3.2. Land response to CDR

The net carbon flux from the atmosphere to the land is denoted as net biome production (NBP), and it is given by the carbon uptake of vegetation through photosynthesis (gross primary production, GPP) minus the losses of carbon to the atmosphere through autotrophic respiration (RA) and heterotrophic respiration (RH), as well as from ecosystem disturbances (DIS) such as fires, with positive/negative values indicating carbon sequestration/release by land. Fig. 6a illustrates that the evolution of NBP in the CDR scenarios closely follow the baseline *SSP5-3.4* scenario. Initially, NBP increases until 2045 during the high emission phase, reaching up to 12 $GtCO_2$/year. This rise is followed by a decrease until 2065, which can be due to sustained high emissions stressing plant systems and consequently reducing NBP. As more CDR implementation is considered in the scenario itself, NBP increases again from 2065 to 2080, before experiencing a further decline towards the end of the century. Fig. 6b shows the cumulative NBP differences from *SSP5-3.4*. In the simultaneous SSP5-3.4-BECCS-OAE, the changes combine linearly, with a value of -15 Pg C in 2100. The cumulative carbon uptake in a scenario where land use is modified to accommodate more bioenergy crops has less CO_2 uptake by land than SSP5-3.4. The decline in NBP from 2060 onwards could be arising from the reduction in atmospheric CO_2 concentrations happening simultaneously. In the OAE simulation, NBP remains closer to the baseline with a smaller reduction of around -4 PgC cumulative by 2100. The combined scenario, *SSP5-3.4-BECCS-OAE* sees the largest reduction in NBP, of almost -16 PgC by 2100. The spatial pattern of the NBP response is similar in all three simulations (Fig. 11), with the magnitudes being stronger in the combined OAE and BECCS case. A certain level of noise is seen due to the relatively small magnitudes of change overall in the carbon cycle.

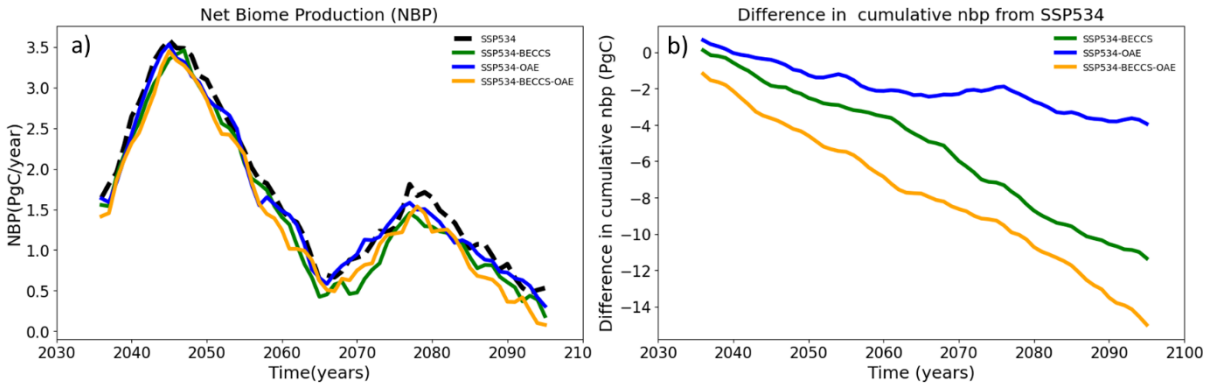

Figure 10: (a) 12-year running mean timeseries of projected uptake of global land NBP (CO_2 taken up by land, atmosphere-land CO_2 flux) in different simulations (PgC / year) (b) change in cumulative NBP with respect to the SSP5-3.4 simulation (PgC).

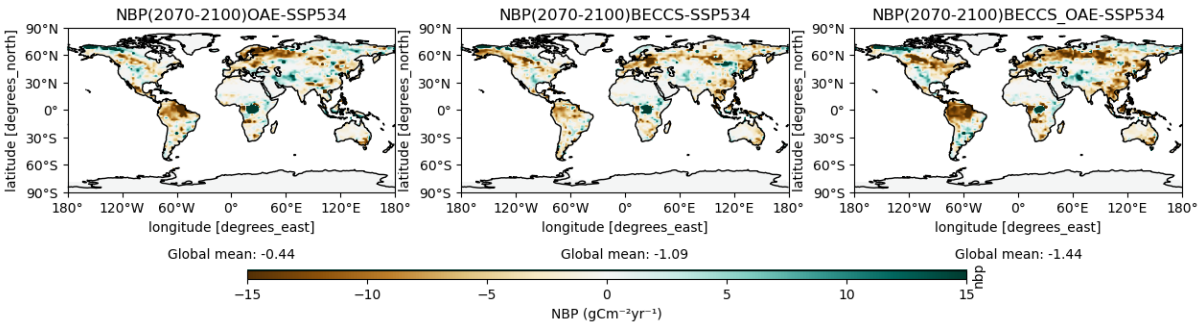

Figure 11: Spatial distributions of NBP (gC/m2/year) over the globe in long-term (2070–2100) periods under the SSP5-3.4-OAE, SSP5-3.4-BECCS and SSP5-3.4-BECCS-OAE scenarios with respect to the SSP5-3.4 scenario.

Until around 2055, there is an increase in the Net Primary Productivity (NPP, NPP = GPP minus RA) (Fig. 12), as the atmospheric CO_2 concentrations are increasing and peaking in SSP5-3.4. However, beyond that NPP steadily decreases, ultimately reaching a value by the end of the century that is similar to the NPP observed in 2030, implies a potential stabilization of primary productivity. The OAE simulation largely follows the same curve, with a somewhat lower NPP, of around 2-3 PgC / year over the second part of this century. This gives an almost nea-linear cumulative decrease in NPP, ending at around -24PgC by 2100 (Fig. 12b). For BECCS on the other hand, the NPP is higher than SSP5-3.4 for most of the simulation. Sugarcane is an energy dense crop type, highly efficient at taking up carbon, with higher yields than the crop types that were replaced. The peak in NPP in the BECCS simulation happens later that the other scenarios, and occurs at a point where the BECCS deployment has increased significantly in the 2060s and at the cusp of the CO2 concentrations, before they are getting reduced more drastically (Fig. 6). Beyond that when the CO2 concentrations are decreasing more, the NPP in the BECCS case also start to decline, but remains mostly higher throughout the deployment period with a cumulative NPP increase of 5 PgC by 2100. In the combined simulation, we see that NPP is largely dominated by the BECCS effect of cultivating high-yield sugarcane. The response in NPP is not linear in the combined simulation, and the NPP remains higher than or the same as SSP5-3.4 until 2070, and the 2100 cumulative value is of -5 PgC.

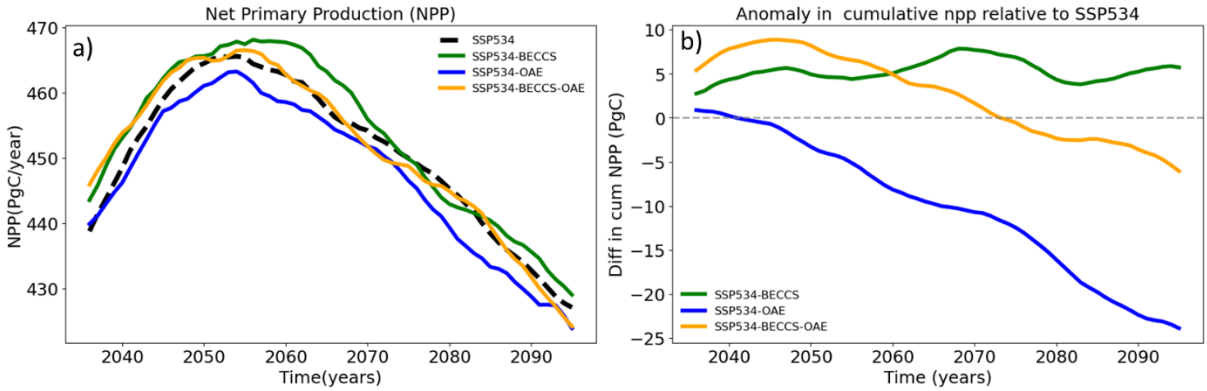

Figure 12: Time series of NPP from each simulation (PgC / year) (a), and (b) cumulative change in NPP with respect to the SSP5-3.4 simulation (PgC).

The spatial distribution of the NPP changes over the last three decades of the simulations reveal the highest increase in NPP in the tropical and subtropical regions with sugarcane plantations in the BECCS and combined BECCS and OAE simulations (Fig. 13). Tropical sugarcane is as expected the strongest driver of the NPP changes seen in the simulations. The OAE case sees a general decrease in NPP over land, with some patchiness, which is more likely 'noise' due to the small forcings applied to the model in this case. The pattern of change in the combined BECCS and OAE case is predominantly dominated by same features seen in the BECCS case.

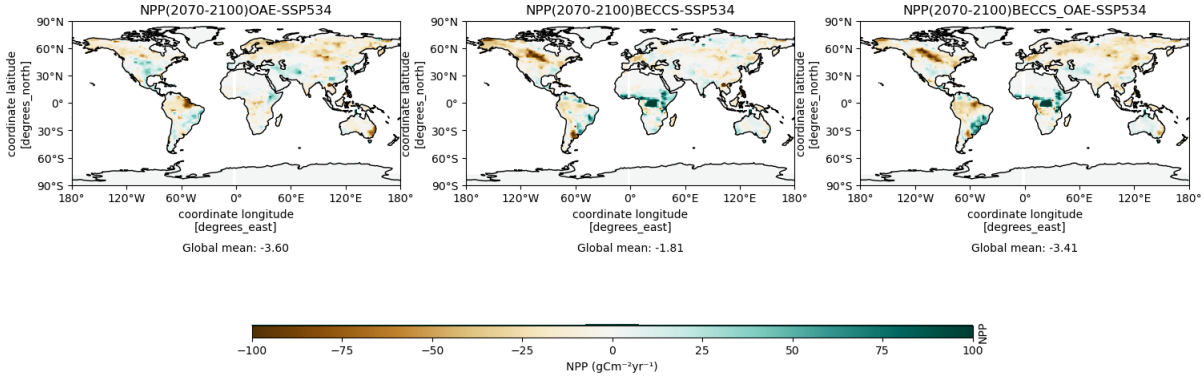

Figure 13: Spatial distributions of NPP changes (gC/m2/year) over the period 2070–2100 for the SSP5-3.4-OAE, SSP53.4-BECCS and SSP5-3.4-BECCS-OAE scenarios compared to the SSP5-3.4 baseline scenario.

The Above Ground NPP (AGNPP) from the additional areas of sugarcane plantations are seen in Fig. 14. The carbon uptake by the sugarcane crops is largely unaffected by the OAE deployment and the sugarcane yield remains as good as the same in both the BECCS and the combined BECCS and OAE simulations. In both cases the AGNPP is of almost 8 PgC per year at the end of the century, which is roughly one quarter of the total AGNPP from all crops.

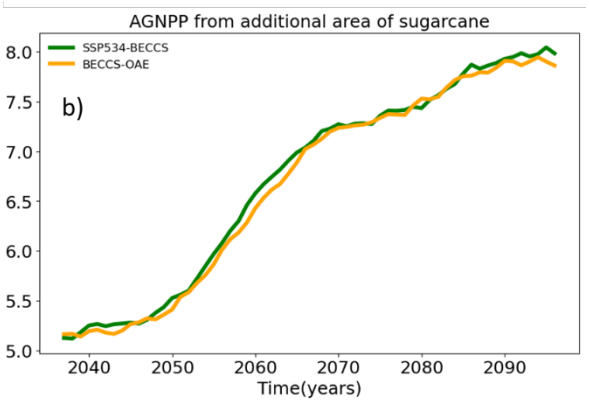

Figure 14: AGNPP from the additional sugarcane areas in the BECCS (green) and BECCS-OAE (orange) simulations (PgC / year).

Gross Primary Production (GPP) and Ecosystem Respiration (ER) exhibit similar patterns to the ones observed for NPP (Fig. 15 and 16). In the *SSP5-3.4-BECCS* simulation, both GPP and ER are consistently higher relative to the baseline *SSP5-3.4* throughout the century. Conversely, the OAE

scenario shows lower GPP and ER values compared to the *SSP5-3.4* baseline, with the difference magnifying over time and reaching its maximum by the end of the century.

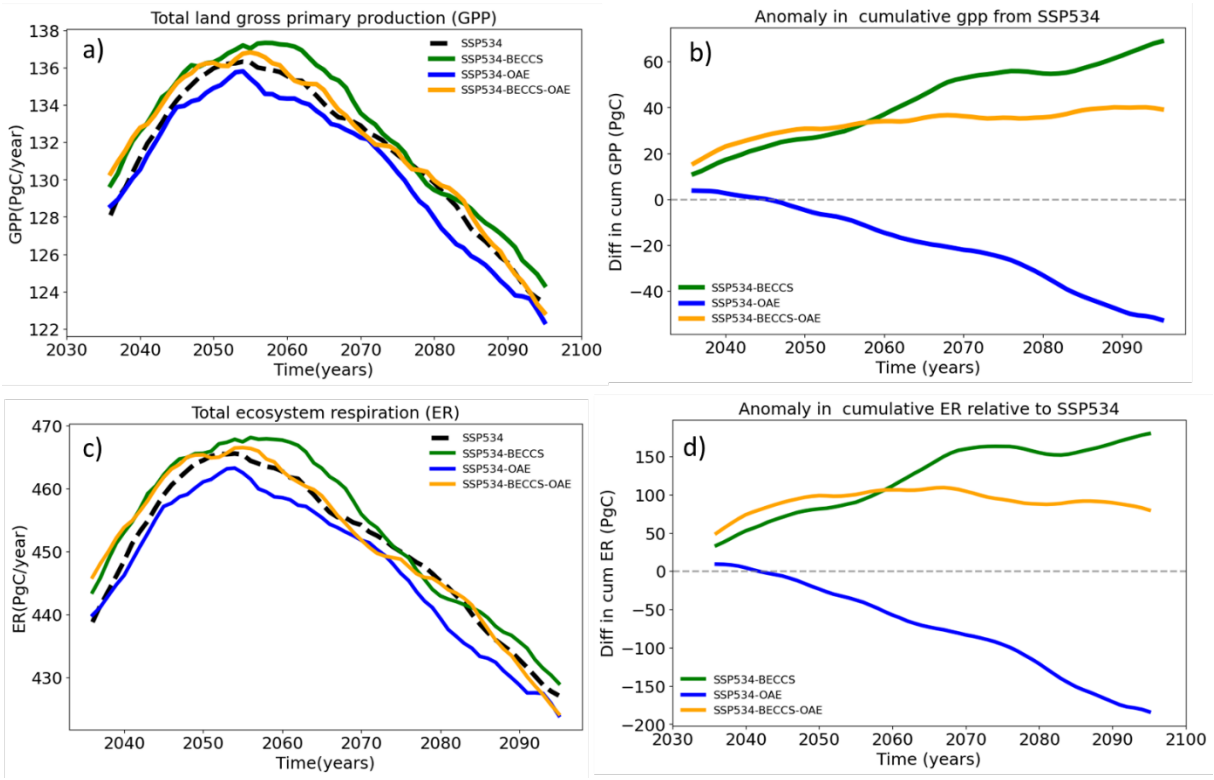

Figure 15: Time series of (a) Gross primary production (PgC / year) (b) cumulative change in Gross primary production with respect to SSP5-3.4 (PgC), c) Ecosystem Respiration (PgC / year), and (d) cumulative change in ecosystem respiration compared to SSP5-3.4 (PgC).

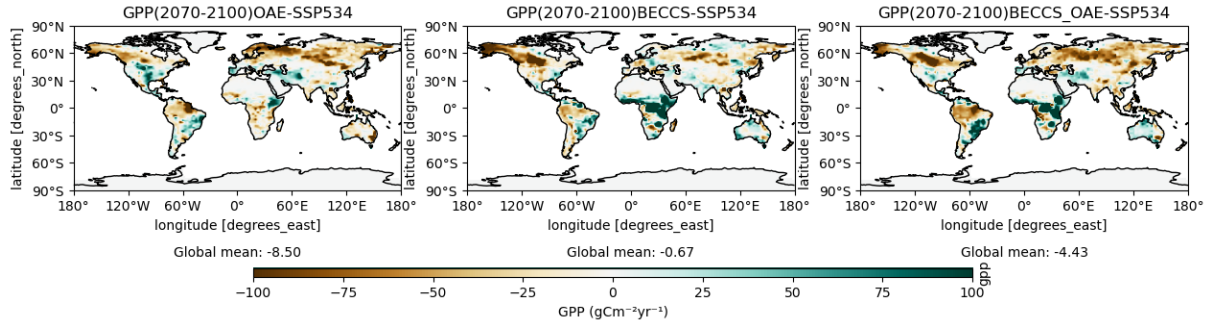

Figure 16: Mean change in GPP (gC m^{-2} $year^{-1}$) over the years 2070–2100 in SSP5-3.4-OAE, SSP5-3.4-BECCS and SSP5-3.4-BECCS-OAE scenarios compared to the SSP5-3.4 scenario.

Total vegetation carbon exhibits an upward trajectory from 2035 to 2060, followed by a minor dip around 2070, before increasing again until 2100 (Fig. 17). The magnitude of increase post-2070 is smaller in CDR scenarios as the CDR methods are increasing in deployment and carbon in the atmosphere is lowered, with the combined BECCS and OAE simulation showing the lowest increase. With regards to soil carbon, BECCS deployment can entail T substantial land-use changes and influence soil carbon dynamics through mechanisms such as changes in biomass input and alteration in decomposition rates. These processes might limit the potential for soil carbon

accumulation, thereby explaining the lower increases observed in SSP5-3.4-BECCS and SSP5-3.4-BECCS-OAE simulations (Table 3).

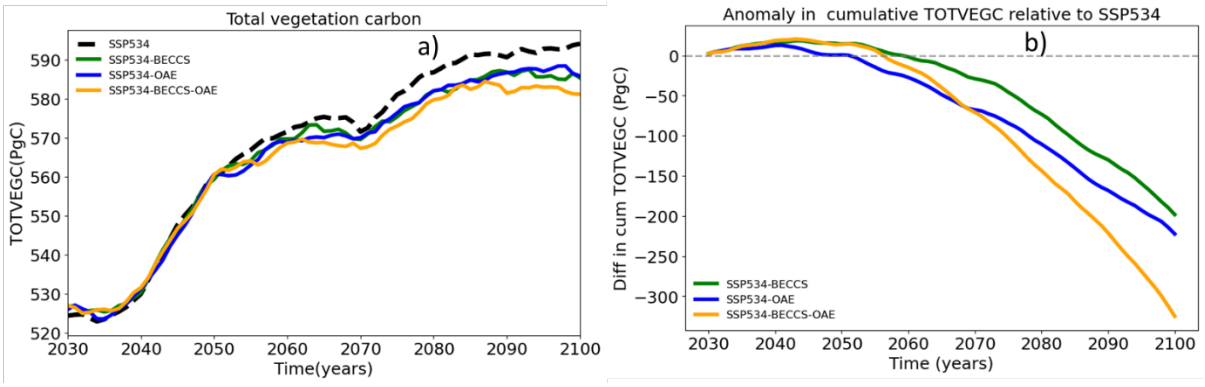

Figure 17: Timeseries comparison of (a) total vegetation carbon (PgC / year), and (b) change in cumulative total vegetation carbon with respect to SSP5-3.4 (PgC).

Table 3: Summary of response in land variables at 2100, reduction relative to SSP534 baseline at 2100, cumulative differences, and 2070 – 2100 mean changes.

Variable	Simulation	Value at 2100	Reduction at 2100 wrt SSP534 at 2100	Cumulative diff at 2100	Reduction in mean 2070-2100 relative to SSP534
NBP PgC/year	SSP534	0.76			
	BECCS	-1.16	-1.92	-13.62	-1.09
	OAE	-0.59	-1.35	-6.62	0.44
	BECCS-OAE	0.08	-0.67	-17.63	-1.44
NPP (PgC)	SSP534	53			
	BECCS	51	-1.6	3.5	-1.8
	OAE	51	-1.75	-28	-3.6
	BECCS-OAE	51.7	-1.33	-11	-3.4
TOTSOILC (PgC)	SSP534	2596.8			
	BECCS	2593.5	-3.3	-135.4	-16.4
	OAE	2599.1	2.25	60.8	17.01
	BECCS-OAE	2593.06	-3.75	-194.9	-21.6
TOTVEGC (PgC)	SSP534	594			
	BECCS	585.3	-8.81	-198	-26.9
	OAE	585.8	-8.29	-222	-35.3
	BECCS-OAE	581.16	-12.98	-324	-39.9

3.3 Ocean response to CDR

The response in sea surface temperatures (SSTs) compared to SSP5-3.4 is comparable to what was seen in the near surface air temperatures (Fig. 18). The SSTs are lower in the last four decades of the century, when the CDR application is stronger. The SST changes are however rather small, with a -0.15 achieved at the most, in the OAE simulation. The BECCS SSTs are very close to the baseline simulation throughout.

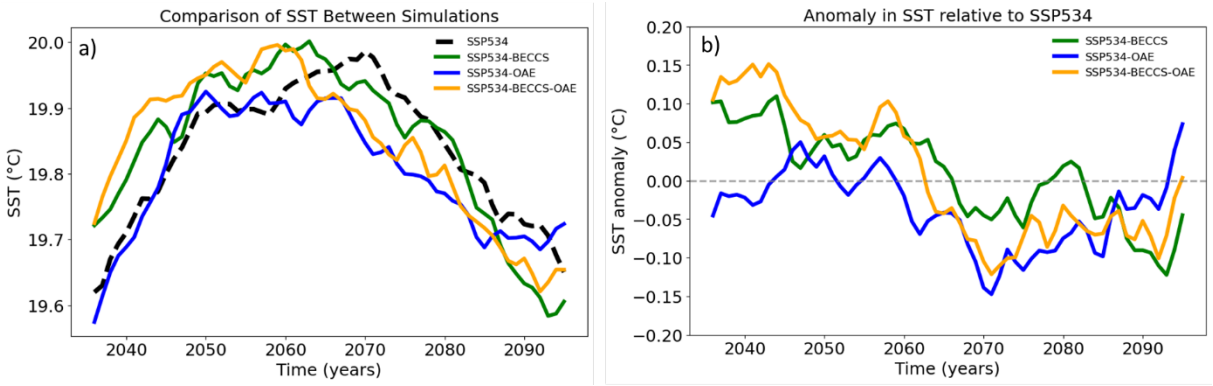

Figure 18: Comparison of (a) 12-year rolling mean global average sea surface temperature (°C), and (b) Difference in SST with respect to the baseline simulation SSP5-3.4.

The air – sea flux of carbon shows a simultaneous peak in all simulations around 2040 with a reduction afterwards as the atmospheric CO2 concentrations are going down (Fig. 19). There is a clear increase in the carbon flux from the atmosphere to the ocean in the OAE case, with an increase of about 0.2 PgC per year by 2100 and a cumulative uptake of 20 PgC. On the other hand, the BECCS deployment results in a net decrease in the carbon uptake in the oceans, as more carbon is taken up by the land, leaving less carbon available for the oceans to take up. Cumulative change in the BECCS simulation is of -14 PgC, and the net in the combined BECCS and OAE simulation is linearly additive. The BECCS simulation shows a small reduction more or less evenly distributed across the oceans.

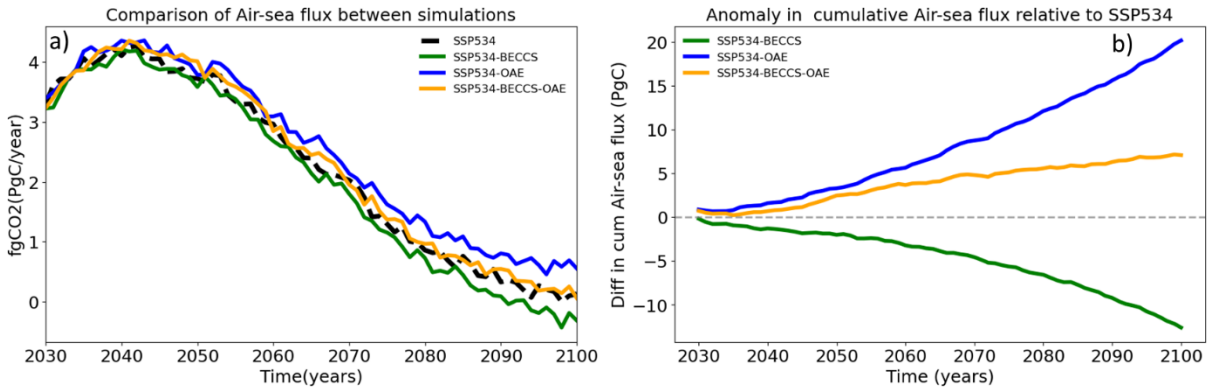

Figure 19: Timeseries of air – sea flux of carbon in each simulation (PgC / year) (a), and the cumulative difference from SSP5-3.4 (PgC) (b).

The spatial distribution of the air – sea carbon flux changes reveal a strong change in the OAE application regions (Fig. 20), with also some increases more widely across the Nort Pacific. This pattern is also evident in the combined BECCS and OAE case.

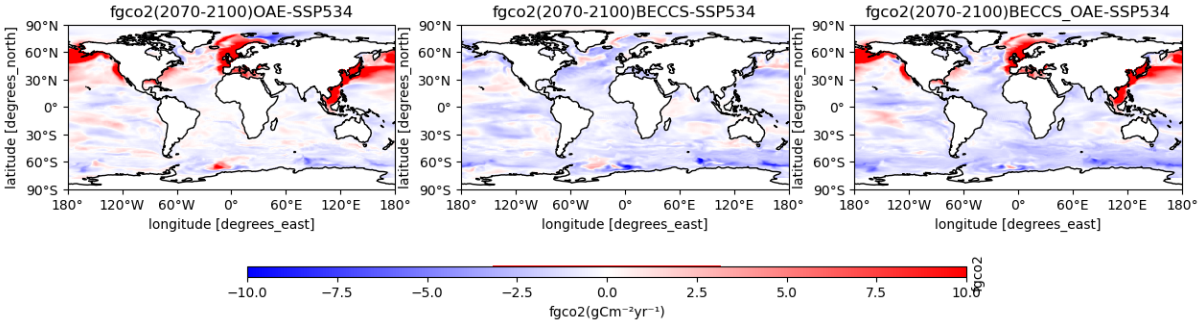

Figure 20: Spatial distributions of changes to the air – sea carbon flux (gC m^{-2}) over the period of 2070–2100 for SSP5-3.4-OAE, SSP5-3.4-BECCS and SSP5-3.4-BECCS-OAE scenarios compared to the SSP5-3.4 scenario.

The partial pressure of CO_2 in the surface ocean is reduced in all the CDR simulations (Fig. 21). There is less dissolved CO_2 in the surface waters when the atmospheric CO_2 concentrations go down and OAE is more effective at reducing the pCO2. The partial pressure is the most reduced in the OAE deployment areas (Fig. 22). There is a cumulative change of -350 - -400 µatm in the OAE and BECCS cases and -700 µatm in the combined one. As to be expected the distribution of change is even across the global oceans in the BECCS simulation (Fig. 22).

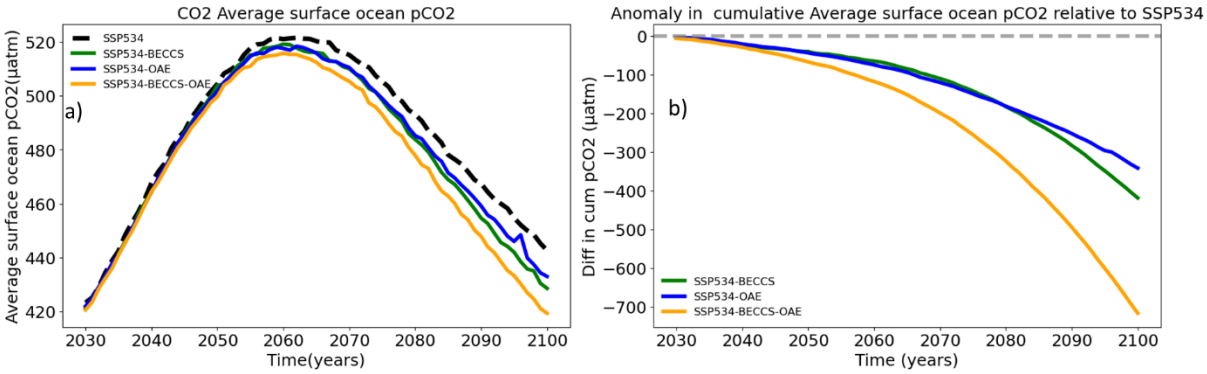

Figure 21: Comparison of (a) global mean pCO2 (µatm), and (b) cumulative change compared to the baseline simulation (µatm).

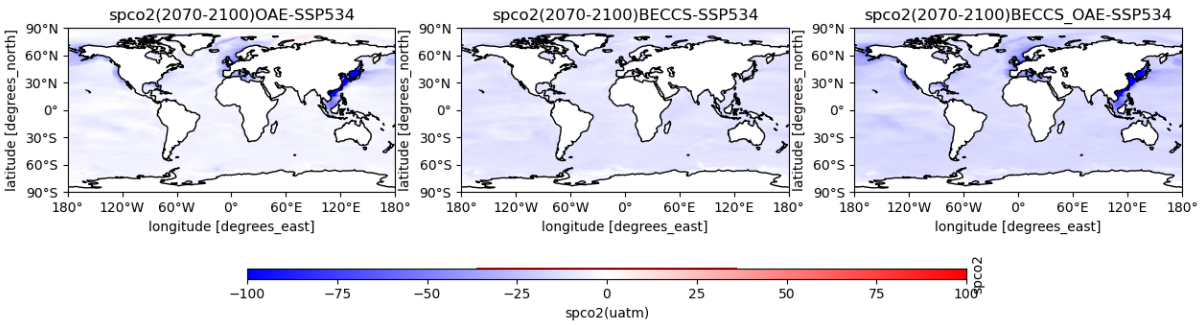

Figure 22: Spatial distributions of change in Surface Ocean pCO2 over the period of 2070–2100 for SSP5-3.4-OAE, SSP5-3.4-BECCS and SSP5-3.4-BECCS-OAE scenarios compared to SSP5-3.4.

Table 4: Summary of ocean variables from the simulations, including the value at 2100, reduction relative to SSP534 baseline at 2100.

Variable	Simulation	Value at 2100	Change in 2100 cf. SSP5-34	Cumulative change by 2100
FgCO2	**SSP534**	**0.132**		
	BECCS	**-0.311**	**-0.444**	**-12.6**
	OAE	**0.556**	**0.423**	**20.17**
	BECCS-OAE	**0.063**	**-0.07**	**7.1**
SST	**SSP534**	**19.5**		
	BECCS	**19.7**	**0.15**	
	OAE	**19.7**	**0.19**	
	BECCS-OAE	**19.6**	**0.10**	
SpCO2	**SSP534**	**442.7**		
	BECCS	**428.59**	**-14.1**	**-418.7**
	OAE	**433**	**-9.7**	**-341.5**
	BECCS-OAE	**419**	**-23.32**	**-717.8**

4. Conclusions

An in-depth analysis of potential climate responses, in particular the carbon cycle, to different CDR methods individually deployed and combined is presented in this Deliverable 4.8 report. We analysed simulations performed with NorESM2 where BECCS is deployed with sugarcane as feedstock, and OAE is deployed within the EEZ of China, EU and the US, and a simulation where both are deployed at the same time with a ramp up throughout the century.

Atmospheric CO_2 concentration changes experience the largest reduction in the combined BECCS and OAE scenario, which turned out to essentially be the sum of the reductions achieved by each method individually. Long-term mean temperature changes at the end of the century show only slight reductions, on the order of less than 0.5°C, in both individual and simultaneous CDR scenarios. In the BECCS simulation, biogeophysical feedbacks are countering the biogeochemical effects, leaving this method less effective at cooling temperatures, but more effective at removing carbon from the atmosphere.

As for the land response, Net Biome Production (NBP) indicates that carbon uptake is twice as high in BECCS compared to OAE, with the simultaneous simulation showing the highest uptake, nearly equaling the sum of the individual BECCS and OAE uptakes. Total soil carbon exhibits emissions in the OAE scenario, uptake in the BECCS scenario, and slightly higher uptake in the combined BECCS-OAE simulation, indicating that the uptake in the simultaneous scenario is not impacted by the emissions from OAE. Total vegetation carbon uptake is nearly identical in the individual BECCS and OAE simulations but increases in the simultaneous BECCS-OAE scenario. The sugarcane yield in the combined BECCS and OAE simulation is unaffected by the OAE deployment, and the terrestrial CDR has the same efficacy no matter is OAE is simultaneously deployed. Other parts of the terrestrial carbon cycle see a reduction in the carbon uptake due to the OAE deployment, however, in the combined case.

The OAE simulation shows higher carbon uptake in the ocean, as expected, whereas BECCS results in a reduction in oceanic carbon uptake due to the lower atmospheric CO_2 concentrations. In the simultaneous BECCS-OAE simulation, there are slight emissions, but these are compensated for by the uptake from OAE.

5. References

Seland, Ø., Bentsen, M., Olivié, D., Toniazzo, T., Gjermundsen, A., Graff, L. S., Debernard, B., Gupta, A. K., He, Y., Kirkevåg, A., Schwinger, J., Tjiputra, J., Karset, H. H., Landgren, O., Liakka, J., Moseid, K. O., & Nummelin, A. (2020). *Overview of the Norwegian Earth System Model (NorESM2) and key climate response of CMIP6 DECK , historical , and scenario simulations*.

Tjiputra, J. F., Schwinger, J., Bentsen, M., L. Morée, A., Gao, S., Bethke, I., Heinze, C., Goris, N., Gupta, A., He, Y. C., Olivié, D., Seland, O., & Schulz, M. (2020). Ocean biogeochemistry in the Norwegian Earth System Model version 2 (NorESM2). *Geoscientific Model Development*, *13*(5), 2393–2431. https://doi.org/10.5194/gmd-13-2393-2020.

Meinshausen, M., Nicholls, Z. R. J., Lewis, J., Gidden, M. J., Vogel, E., Freund, M., Beyerle, U., Gessner, C., Nauels, A., Bauer, N., Canadell, J. G., Daniel, J. S., John, A., Krummel, P. B., Luderer, G., Meinshausen, N., Montzka, S. A., Rayner, P. J., Reimann, S., Smith, S. J., van den Berg, M., Velders, G. J. M., Vollmer, M. K., and Wang, R. H. J.: The shared socio-economic pathway (SSP) greenhouse gas concentrations and their extensions to 2500, Geosci. Model Dev., 13, 3571–3605, https://doi.org/10.5194/gmd-13-3571-2020, 2020.

Muri, H. (2018). The role of large—scale BECCS in the pursuit of the 1.5°C target: an Earth system model perspective. Environmental Research Letters, 13 044010 DOI 10.1088/1748-9326/aab324.

Partanen, Antti-Ilari and Bergman, Tommi (2024) ESM data-set on multiple ocean NET simulations. OceanNets Deliverable, D4.6. OceanNETs, Kiel, Germany, 13 pp. DOI 10.3289/oceannets_d4.6.

Sathyanadh, Anusha and Muri, Helene (2024) Open access dataset of ESM simulations of combined land- and ocean-based NETs. OceanNets Deliverable, D4.7. OceanNets, 11 pp. DOI 10.3289/oceannets_d4.7.

6. Appendix

Table 5: List of land and atmospheric variables, their units and long names

Variable Name Original vs needed	Units	Long name
nbp_glob	Pg C yr^{-1}	Globally integrated air-land CO_2 flux (positive downward)
gpp_glob	Pg C yr^{-1}	Total land gross primary production
cveg_glob	Pg C	total vegetation carbon
csoil_glob	Pg C	total soil organic matter carbon
NPP	Pg C yr^{-1}	net primary production
AGNPP	Pg C yr^{-1}	aboveground NPP
ER	Pg C yr^{-1}	total ecosystem respiration, autotrophic + heterotrophic
RTMT		
xco2atmga	ppm	Global average surface atmospheric mixing ratio of CO_2 (with respect to dry air)
tasga	°C	Global average atmospheric near surface temperature
SST		
fgCO2		Air-sea CO2 flux (positive downward)
SpCO2		Surface ocean pCO2